Electromagnetic Science
vol. 2, no. 1, 0050372, March 2024
https://doi.org/10.23919/emsci.2023.0037

Research Article

Effect of Fe Substitution on Magnetic Properties and Radar Wave Absorption of the Y_2Co_{17} Rare Earth Soft Magnetic Alloy

Chengfa Tu and Liang Qiao

Institute of Applied Magnetism, Key Laboratory for Magnetism and Magnetic Materials of Ministry of Education, Lanzhou University, Lanzhou 730000, China

Corresponding author: Liang Qiao, Email: qiaoliang@lzu.edu.cn.
Received September 19, 2023; Accepted December 15, 2023; Published Online March 13, 2024.

Abstract — The rapid development of information technology leads a demand for high frequency soft magnetic materials with exceptional radar wave absorption properties. A new magnetic material with superior radar wave absorption is explored in this paper. we explored the preparation of $Y_2Co_{17-x}Fe_x$ (x = 0.0, 1.0, 2.0, 3.0) alloy powders using yttrium oxide as a raw material by a low-cost and short preparation cycle reduction-diffusion process. The crystal structure, intrinsic magnetic properties, high frequency magnetism and radar wave absorption of $Y_2Co_{17-x}Fe_x$ (x = 0.0, 1.0, 2.0, 3.0) were investigated. These compounds have a perfect magnetic repair of Y_2Co_{17} and enable the improvement of the overall magnetic properties of $Y_2Co_{17-x}Fe_x$ (x = 0.0, 1.0, 2.0, 3.0) compounds. The $Y_2Co_{17-x}Fe_x$/Polyurethane (PU) (x = 0.0, 1.0, 2.0, 3.0) absorbers were divided in detail using the zero-reflection mechanism. The results show that all $Y_2Co_{17-x}Fe_x$/PU (x = 0.0, 1.0, 2.0, 3.0) absorbers have excellent absorption performance (reflection loss RL is less than −85 dB); in addition, $Y_2Co_{15}Fe_2$/PU absorbers and $Y_2Co_{14}Fe_3$/PU absorbers are superior candidates for S-band materials. In particular, the perfectly matched frequency f_p of the modulated $Y_2Co_{14}Fe_3$/PU absorber is shifted to the L-band (1–2 GHz) where early warning radars are located. The $Y_2Co_{14}Fe_3$/PU absorber has an effective absorption bandwidth of 300 MHz (1.5–1.8 GHz) at a thickness of 5.230 mm. It can also absorb the full L-band at −4 dB, which has rarely been reported.

Keywords — Rare earth soft magnetic alloy, Reduction diffusion, Soft magnetic composites, Zero-reflection condition, Reflection loss.

Citation — Chengfa Tu and Liang Qiao, "Effect of Fe substitution on magnetic properties and radar wave absorption of the Y_2Co_{17} rare earth soft magnetic alloy," *Electromagnetic Science*, vol. 2, no. 1, article no. 0050372, 2024. doi: 10.23919/emsci.2023.0037.

I. Introduction

Nowadays, high frequency electromagnetic radiation has increased dramatically due to the rapid development of a wide range of microwave applications [1]–[6], such as standard radar, satellite and military systems, especially 5G communication technology operating in the S-band [5], [7]. The massive presence of GHz microwaves does not only cause serious electromagnetic interference problems, leading to malfunction or damage to electronic equipment [8]–[12], but also increases health risks for human [13], [14]. There has been a growing interest in absorbers that can have wider absorption bandwidth, greater absorption capacity, higher operating frequency, and lighter mass [15]–[18], leading to a significant need in finding general and effective ways to develop materials with good electromagnetic wave absorption properties in the microwave frequency range [19]–[24].

Thankfully, significant efforts have been made by material scientists to develop wave-absorbing materials [25]–[28], such as carbonyl iron and ferrite have been thoroughly studied. Carbonyl iron [29], a soft magnet, is an excellent wave-absorbing material in the MHz region. Ferrites are considered to be the best candidates for microwave absorbing materials due to their unique combination of magnetic and insulating properties. However, the performance of these materials at GHz is significantly reduced due to the MHz domain wall resonance of the magnetic materials, which limits their overall application [4], [11], [13].

In particular, rare earth-3D transition metal soft magnetic compounds have received widespread attention for

their soft magnetic properties [4], [17], [30], [31], such as high saturation magnetisation M_s and Curie temperature T_c, since the beginning of the 21st century. Soft magnetic composites (SMCs) consisting of micron-sized magnetic particles coated or mixed with insulating materials using powder metallurgy techniques have been shown to exhibit excellent microwave absorption properties in GHz region. Maeda *et al.* reported in 2004 that the $Y_{9.4}Fe_{79.3}B_{11.1}Cu_{0.2}$ composite showed good microwave absorption properties (over 99%) at 39.5 GHz [32]. In 2007, Lian *et al.* showed that the $Nd_2Fe_{14}B/\alpha$-Fe nanocomposite exhibited excellent microwave absorption properties with an reflection loss (RL) less than −20 dB [33]. In recent years, the combination of different compounds with varying properties to create new composites has generated significant technical interest [34], [35]. The addition of a second phase has shown to significantly improve the magnetoelectric properties of resulting composites, leading to remarkable achievements in material parameters, magnetic properties, and wave absorption capabilities [36]. In recent years, there have been noteworthy progress in the development of composites with improved material parameters, magnetic and wave absorption properties. Qiao *et al.*'s study [37] on Sm-substituted $(Nd_{1-x}Sm_x)_2Fe_{14}B$/paraffin composites showed excellent microwave absorption properties, with an average reflection loss (RL) of less than 10 dB at 6–18 GHz. Meanwhile, Yang *et al.* demonstrated a maximum RL of 55.1 dB and a qualified bandwidth (QB) of 3.7 GHz (12.7–16.4 GHz) for the $Sm_{1.5}Y_{0.5}Fe_{15.5}Si_{1.5}$-paraffin complex [38]. However, the majority of these absorbing materials operate in the X- or Ku-band, and there has been little reported on the lower frequency bands of S- and C-band. Recently, the reduction-diffusion process has been explored to produce alloyed materials, which can effectively reduce the cost of preparing alloyed materials compared to conventional melting processes, by using metal oxides as raw materials [4], [17], [39]. This process has many advantages in industrial production, such as short production cycles, low energy consumption and high cost-effectiveness and there have been few articles on reduction-diffusion synthesis for the Y_2Co_{17} alloy.

Hence, we have utilized a low-cost and short preparation cycle reduction-diffusion process to prepare $Y_2Co_{17-x}Fe_x$ alloy powders using yttrium oxide as a raw material, which is different from the conventional melting process. In order to adjust the dielectric properties of the Y_2Co_{17} alloy powder, we prepared $Y_2Co_{17-x}Fe_x$ $(x = 0.0, 1.0, 2.0, 3.0)$ alloy/polyurethane (PU) soft magnetic composite materials by ultrasonic compounding and hot pressing. Our report includes the crystal structure and the magnetic properties of $Y_2Co_{17-x}Fe_x$ $(x = 0.0, 1.0, 2.0, 3.0)$, and the high-frequency properties of their polyurethane composites. We found that substituting Fe can tune the intrinsic magnetic, dielectric, and microwave absorption properties of the $Y_2Co_{17-x}Fe_x$ $(x = 0.0, 1.0, 2.0, 3.0)$/PU composites. The reflection loss perfect match peak frequency (f_p) decreases with increasing Fe content, in agreement with the variation of natural frequencies measured by the magnetic spectrum. We also discuss the conditions for the exact match of $Y_2Co_{17-x}Fe_x$ $(x = 0.0, 1.0, 2.0, 3.0)$/PU absorbers with different amounts of Fe replacement, and match the interfacial reflection model. A comprehensive study yielded perfect absorbing properties for Y_2Co_{17}/PU and $Y_2Co_{16}Fe_1$/PU absorbers in C-band, while $Y_2Co_{15}Fe_2$/PU and $Y_2Co_{14}Fe_3$/PU absorbers are excellent candidates in L-band.

II. Experiment

1. Synthesis of $Y_2Co_{17-x}Fe_x$ compounds

The $Y_2Co_{17-x}Fe_x$ powder was synthesized by a reduction-diffusion process, as shown in Figure 1. Firstly, Y_2O_3 (purity

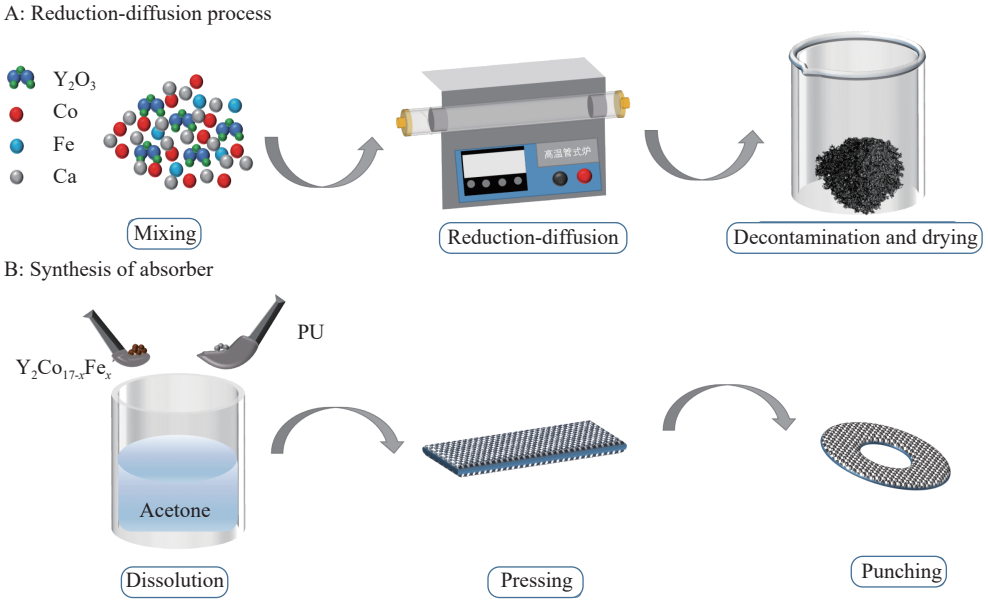

Figure 1 Synthesis of the $Y_2Co_{17-x}Fe_x$ powder and the $Y_2Co_{17-x}Fe_x$ powder-polyurethane absorber.

99.99%, 3 μm), Co powder (purity 99.9%, 3–5 μm), carbonyl iron powder (spherical, purity 99.9%, 3–5 μm) and Ca (purity 99%, 3 mm) were mixed in an argon atmosphere for 8 hours. An excess of about 5wt% Y_2O_3 was used to compensate for Y evaporation. Then the homogeneous mixture was placed in a tube stove and heated at 800 ℃ for 3 hours under an argon atmosphere of 200 ml/min, followed by heating at 1100 ℃ for 3 hours to obtain a mixture of $Y_2Co_{17-x}Fe_x$ and calcium oxide powder.

After the reduction-diffusion process, the samples were crushed to 200 mesh and washed with a 5wt% ammonium acetate solution to remove impurities such as residual Ca and formed CaO. The powder was then immediately washed again with ethanol and dried in a vacuum drying oven at 50 ℃ for 4 hours to obtain $Y_2Co_{17-x}Fe_x$ powder. To measure the microwave absorption properties, the pellets (20–50 μm) were crushed for 3 hours using the ball milling method. The milling balls had a diameter of 2 mm and the mass ratio of pellets to balls was 1:20. To prevent oxidation, both pellets and grinding balls were soaked in hexane during the ball milling process. Oleic acid, 2% of the weight of the pellets, was used as an auxiliary for ball milling.

2. Preparation of the absorbers

Polyurethane (PU) was used as the matrix polymer to prepare the composite as shown in Figure 1. Specifically, firstly, PU was added to a beaker with an appropriate amount of acetone under sonication. Secondly, $Y_2Co_{17-x}Fe_x$ powder was added after the PU was completely dissolved and stirred under ultrasonication until the acetone was completely evaporated to obtain the $Y_2Co_{17-x}Fe_x$ powder-polyurethane mixture. The mass ratio of ground particles to polyurethane is 1:5. Finally, the $Y_2Co_{17-x}Fe_x$ powder-polyurethane composite was compressed into a toroidal shape with inner diameter of 3.04 mm and outer diameter of 7.00 mm under 5 MPa.

3. Characterization

The crystal structure of the samples was identified by X-ray diffraction (XRD) (Philips, $Cu_{K\alpha}$ radiation). And the static magnetism of the sample was measured by vibrating sample magnetometer (VSM, Lake Shore 7304) under an applied magnetic field of 20 kOe at room temperature (about 300 K). The size and morphology of $Y_2Co_{17-x}Fe_x$ ($x = 0.0, 1.0, 2.0, 3.0$) particles were observed by scanning electron microscopy (SEM, TESCAN MIRA3) imaging. The permittivity and permeability of the samples are measured by a vector network analyzer (VNA, Agilent N5247A) in the 0.1–18 GHz range.

III. Results and Discussions

1. Structural characterization and and microstructure of $Y_2Co_{17-x}Fe_x$ (x = 0.0, 1.0, 2.0, 3.0) compounds

All XRD peaks of the $Y_2Co_{17-x}Fe_x$ compounds ($x = 0.0, 1.0, 2.0, 3.0$) in the patterns can be clearly indexed to 2:17 tetragonal crystal structure [40] (PDF:#18-0434) as shown in Figure 2(a). These patterns essentially do not change, proving that the Fe atom replacement does not affect the compound's crystal structure. Additionally, every pattern has a strong peak, which shows that every sample has a good crystallization. However, the XRD peaks of the compounds are pushed towards the lower 2θ direction with the increase of Fe concentration because the Fe atom is bigger than the Co atom, as seen in Figure 2(b), which shows the enlarged section of the XRD patterns.

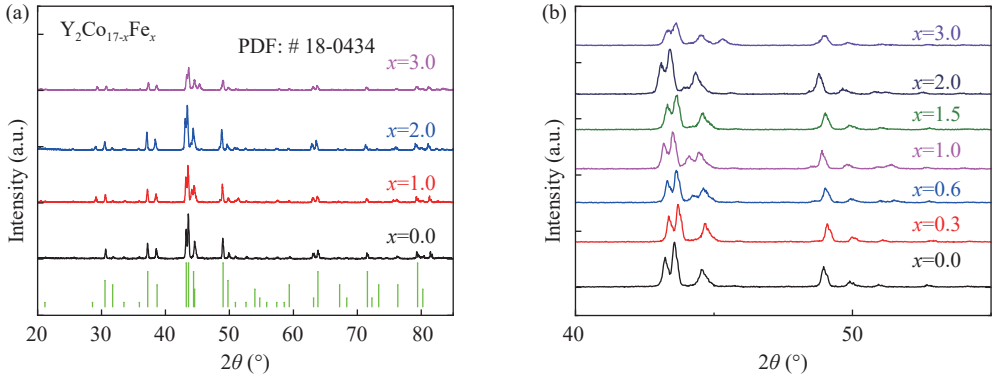

Figure 2 (a) XRD patterns of $Y_2Co_{17-x}Fe_x$ ($x = 0.0, 1.0, 2.0, 3.0$) compounds; (b) Enlarged XRD patterns of $Y_2Co_{17-x}Fe_x$ ($x = 0.0, 1.0, 2.0, 3.0$) compounds.

An intriguing physical phenomena is the micro-shift of the crystal diffraction peaks caused by the replacement of iron. Further in-depth analysis of the XRD diffraction was necessary for this cause. The XRD pattern after iron substitution was optimised with FullProf and the results of this optimisation are shown in Figure 3. The optimisation shows that the experimentally measured data and the theoretically calculated values are in good agreement, indicating that there is not much stray phase generation.

With the increase of x, main characteristic peaks of $Y_2Co_{17-x}Fe_x$ ($x = 0.0, 1.0, 2.0, 3.0$) compounds shift to the lower angle, implying a change in the lattice parameters and unit cell volume with x. The corresponding lattice parameters c, a, unit cell volume V and c/a of the tetragonal phase

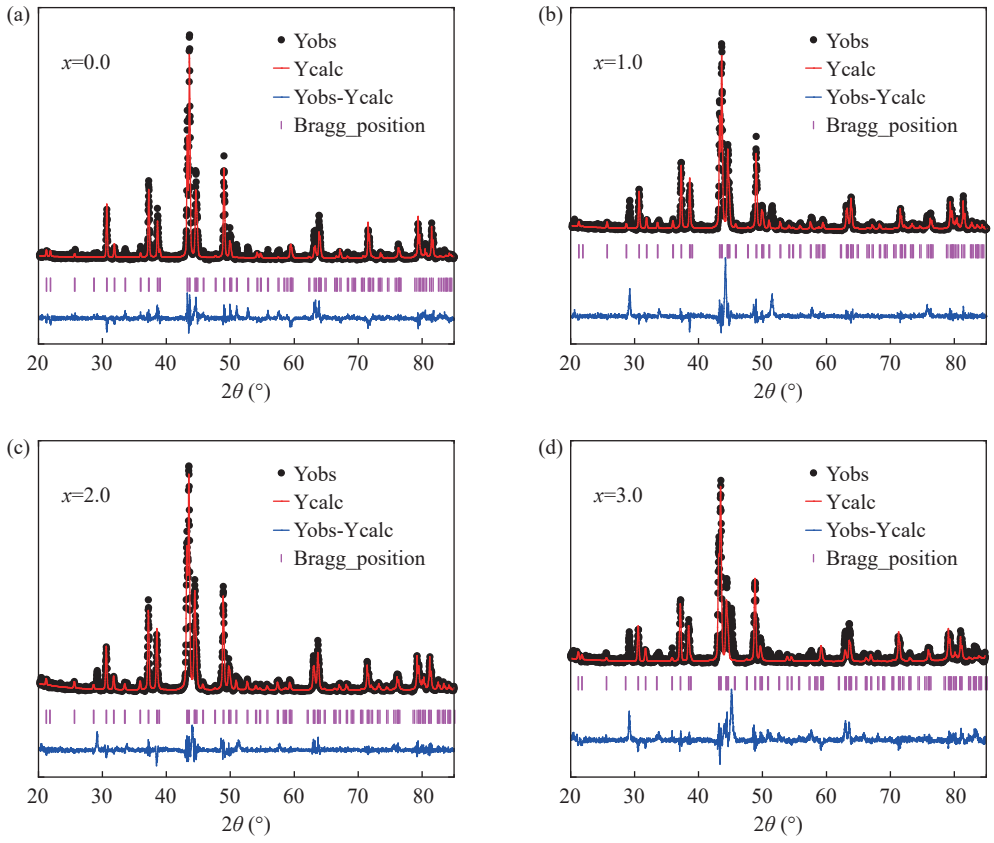

Figure 3 Refined RT XRD patterns of $Y_2Co_{17-x}Fe_x$ ($x = 0.0, 1.0, 2.0, 3.0$) compounds.

were determined by Rietveld refinement and are plotted in Figure 4. With a rise in the Fe content, which may be fused linearly, the valve of c, a, and V increases monotonically. According to empirical alloy theory, the volume of Y_2Fe_{17} is 15%–20% smaller than that of Y_2Co_{17}, which accounts for the rise in lattice constant [41]. Figure 4 amply demonstrates that the steady increase in cell parameters a and c with increasing numbers of substituted Fe atoms leads to an increase in cell volume and coincides with the shift of the XRD diffraction peak in the low-angle direction of 2θ.

Figures 5(a)–(d) show SEM images of the original $Y_2Co_{17-x}Fe_x$ ($x = 0.0, 1.0, 2.0, 3.0$) powders. As can be seen in Figure 5, before ball milling, the sample exhibits an irregular shape with an average particle size of approximately 15 μm gradually. It is well known that metallic materials show a significant skin effect at high frequency, resisting electromagnetic waves to transmit into the inner part of the materials. To reduce the eddy current loss of the material at high frequency, we reduced the size of the material by high-energy ball milling and embedded it into insulating materials such as polyurethane.

As seen in Figure 6, the morphology of the sample has

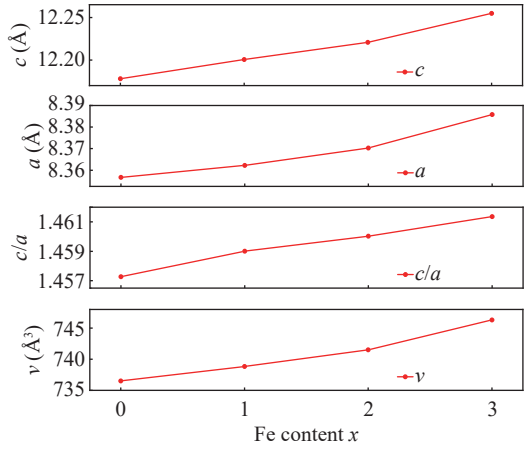

Figure 4 Fe-concentration dependence of lattice parameters c, a, unit cell volume V and c/a of the 2:17 phase.

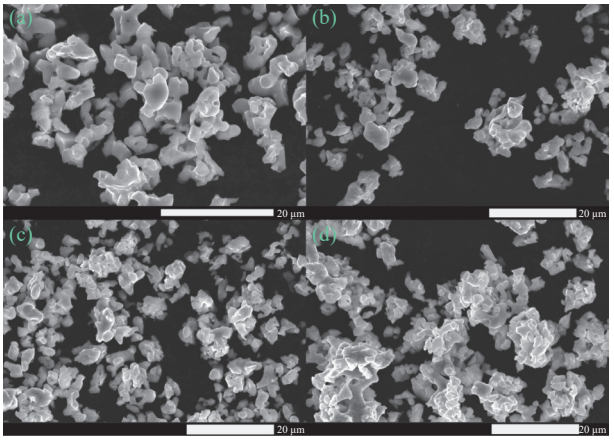

Figure 5 (a)–(d) SEM images of raw $Y_2Co_{17-x}Fe_x$ ($x = 0.0, 1.0, 2.0, 3.0$) compounds.

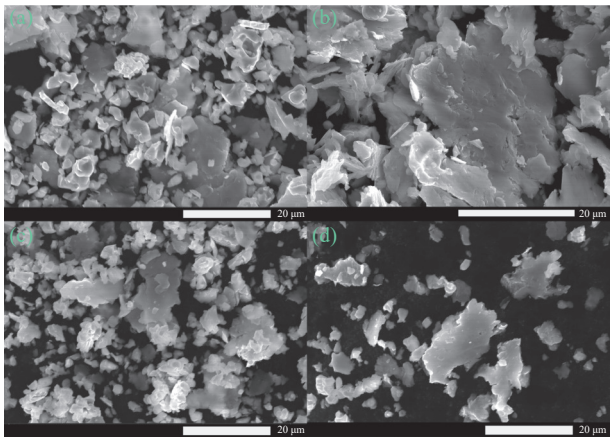

Figure 6 (a)–(d) SEM images of $Y_2Co_{17-x}Fe_x$ ($x = 0.0, 1.0, 2.0, 3.0$) powder after ball milling.

changed from an irregular spherical sample to a flattened flake after high-energy ball milling, and the large particles with an average diameter of 15 μm gradually transformed into small particles with an approximate length of 3–9 μm and a thickness of 0.2–1 μm. During the ball milling process, these particles become plastically deformed and undergo a welding effect due to the enormous pressure acting on them. This deformation results in the formation of small flake particles, while the welding effect causes a small number of particles to fuse with each other and form multilayered flakes. In general, after high-energy ball milling, the thickness of most particles is less than the skinning depth, which facilitates the reduction of eddy currents and improves microwave absorption performance.

2. Static magnetic properties of $Y_2Co_{17-x}Fe_x$ ($x = 0.0, 1.0, 2.0, 3.0$) compounds

Figure 7(a) depicts the hysteresis loops for $Y_2Co_{17-x}Fe_x$ powders ($x = 0.0, 1.0, 2.0, 3.0$) in the presence of a 20 kOe applied magnetic field at RT. The enlarged portion of the hysteresis line is shown in the inset. The magnetization of the $Y_2Co_{17-x}Fe_x$ ($x = 0.0, 1.0, 2.0, 3.0$) powders rises substantially with increasing elemental Fe, as illustrated in Figure 7(a). We see that all of the $Y_2Co_{17-x}Fe_x$ ($x = 0.0, 1.0, 2.0, 3.0$) powders magnetization curves show unsaturated features. The magnetization curves for the measured field parallel to the alignment direction of the $Y_2Co_{17-x}Fe_x$ ($x = 0.0, 1.0, 2.0, 3.0$) powders are shown in Figure 7 (b). It follows the same principle as Figure 7(a) in that the intensity of the magnetization varies with the amount of Fe content substitution and that not all samples are magnetized to saturation.

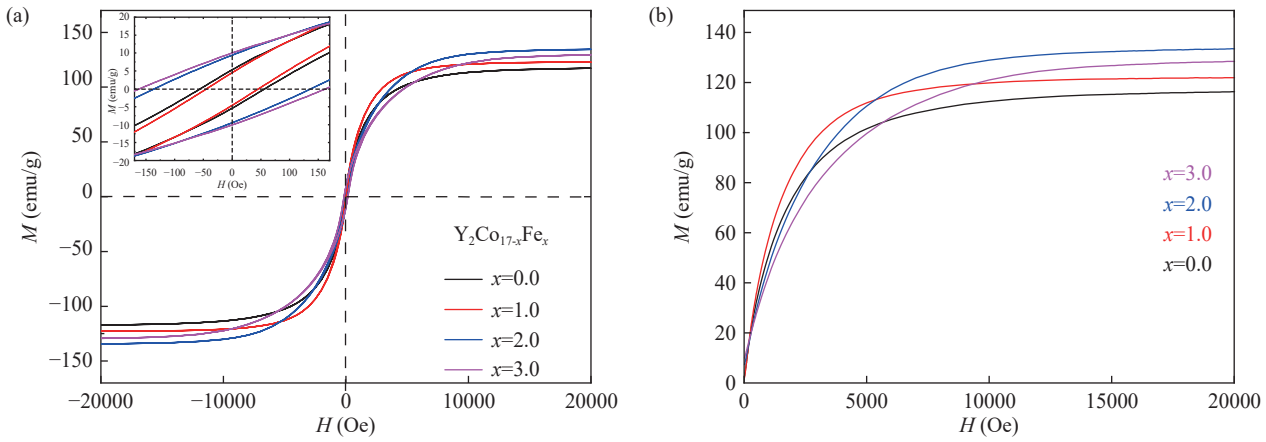

Figure 7 (a) Hysteresis loops of $Y_2Co_{17-x}Fe_x$ ($x = 0.0, 1.0, 2.0, 3.0$) compounds at room temperature (The inset shows the enlarged portion of the hysteresis line of $Y_2Co_{17-x}Fe_x$ ($x = 0.0, 1.0, 2.0, 3.0$) compounds); (b) Initial magnetisation curve of $Y_2Co_{17-x}Fe_x$ ($x = 0.0, 1.0, 2.0, 3.0$) compounds at room temperature.

In order to fit and determine the saturation magnetization intensities of all samples, convergence saturation quantification was used. The convergence saturation law was then written as follows [42]:

$$M = M_s\left(1 - \frac{a}{H} - \frac{b}{H^2} - \cdots\right) + kH \tag{1}$$

where, M denotes the magnetization, M_s denotes the saturation magnetization, a and b are the magnetization parameters, and H is the magnitude of the applied field. Therefore, Figure 8 summarises the value of the saturation magnetisation (M_s) obtained by converging to the saturation law, the value of the coercivity (H_c) read on the hysteresis line. As the substitution of Fe increases, the value of saturation magnetisation initially is 117.15 emu/g for $x = 0$; increases to 122.83 emu/g for $x = 1$; then increases to a maximum value of 134.48 emu/g for $x = 2$; and finally decreases to 129.45 emu/g for $x = 3$. Thus, the M_s values of the $Y_2Co_{17-x}Fe_x$ composites increase first and then decrease with increasing Fe content. This coincides with Zhon's work [43]. In addition, there is a slight decrease in the value of H_c at $x = 1.0$ as the iron substitution increases, followed by a significant increase. This may be attributed to changes in magnetic anisotropy and lattice distortions due to the substitution of Fe atoms.

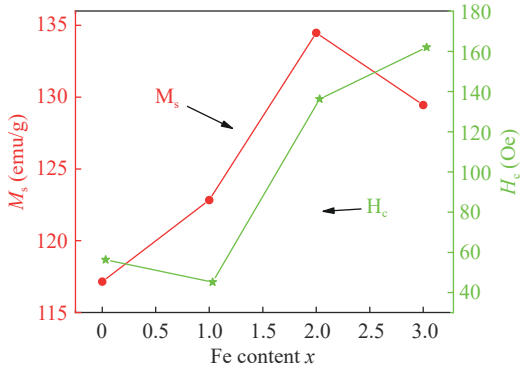

Figure 8 The extracted H_c from the hysteresis loops and the saturation magnetisation M_s obtained by convergence saturation law.

3. Microwave absorbing properties

1) The electromagnetic parameters of wave absorbers

In the field of radar wave absorption, it is well known that the complex permeability and complex permittivity are crucial for the design of absorbers, both in terms of electromagnetic loss theory and interference phase extinction theory. Figure 9 shows the frequency dependence of the complex permeability ($\mu = \mu' - i\mu''$) and permittivity ($\varepsilon = \varepsilon' - i\varepsilon''$) for the $Y_2Co_{17-x}Fe_x$/PU composites in the range of 0.1–8 GHz. As shown in Figure 9(a), the real part of the permeability (μ') does not change much at 0.1 GHz with the substitution of Fe elements, all concentrated around 2.4. Moreover, the values of all composites decrease gradually with increasing frequency in 0.1–8 GHz. Commonly, magnetic losses occur in magnetic materials under the influence of external fields and are mainly attributed to hysteresis, domain wall resonance, natural resonance and eddy currents. Since the radar wave can be regarded as weakly magnetic, the magnetic loss due to hysteresis is negligible here, while domain wall resonance usually occurs in the MHz range. The contribution of eddy currents can also be considered negligible due to the small particle size of the composite and the insulator matrix. Therefore natural resonances are the principal factor affecting magnetic losses in radar wave absorbing materials. The dependence of the imaginary part of the permeability (μ') and frequency (f) shows that μ' increases with f for all samples from 0.1 to 10 GHz, with a maximum value of μ'_{max} occurring at around 10 GHz and then gradually decreasing at 10–18 GHz. This indicates that the natural resonance frequency of all samples occurs at around 10 GHz, which is beyond the natural resonance frequency of ferrite. From the equation $(\mu_0 - 1) \times f_r = \frac{2}{3}\gamma M_s \sqrt{\frac{H_a}{H_c}}$ [44], we know it is understandable that the samples have a low permeability.

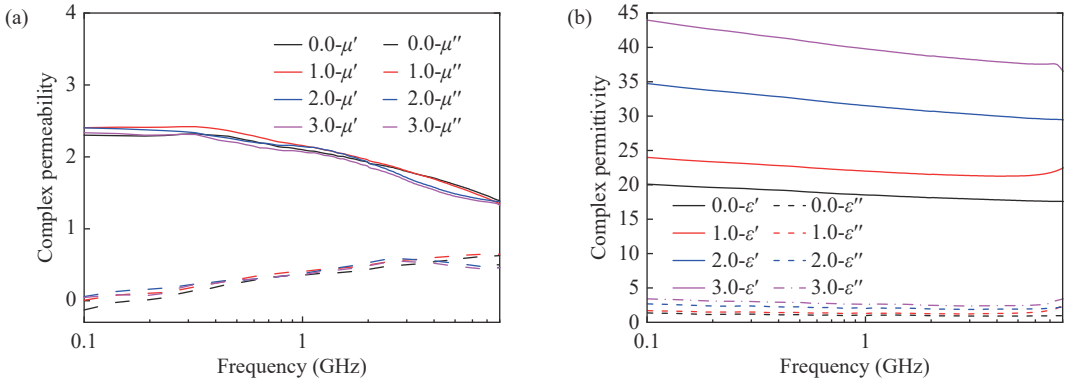

Figure 9 The electromagnetic parameters of the $Y_2Co_{17-x}Fe_x$/PU composites ($x = 0.0, 1.0, 2.0, 3.0$). (a) The complex permeability; (b) The complex permittivity.

For magnetic materials, magnetic parameters are critical for wave absorbers. Similarly, an appropriate complex permittivity are always advantageous for improving electromagnetic impedance matching and enhancing the microwave absorption properties of metallic magnetic materials. From Figure 9(b), it can be seen that for all $Y_2Co_{17-x}Fe_x$/PU composites, the value of the real part of the permittivity (ε') for $x = 0.0$, $x = 1.0$, $x = 2.0$ and $x = 3.0$ composites are 20, 24, 35 and 45 at 0.1 GHz, respectively. Overall, the real part of the permittivity gradually increases as the Fe substitution increases. They have a fluctuation in the high frequencies, which is a measurement error. The imaginary part of the dielectric remains smooth between 0.1 and 18 GHz, which facilitates impedance matching.

2) Zero reflection parameters of wave absorbers

As we all know, the comprehensive requirements for absorbing materials are "thin, light, wide and strong" from the perspective of absorbing materials application, whether it is warship stealth or civil shielding materials. Unfortunately, the existing absorbing theory cannot fully accomplish the comprehensive analysis of the "thinness, lightness, width and strength" of absorbing materials. For this reason, we combine the phase matching conditions and transmission line theory to make the integrated analysis of absorbing materials in the following mathematical expression.

The phase matching condition [45] is expressed as

$$t = \frac{nc}{4f\sqrt{\mu_r \varepsilon_r}}, \quad n = 1, 3, 5, \ldots \tag{2}$$

and the transmission line theory [17], [40] is expressed as

$$Z_{in} = Z_0 \sqrt{\frac{\mu_r}{\varepsilon_r}} \tanh\left(i\frac{2\pi f t}{c}\sqrt{\mu_r \varepsilon_r}\right) \quad (3)$$

$$RL(dB) = 20\mathrm{Log}_{10}\left|\frac{Z_{in} - Z_0}{Z_{in} + Z_0}\right| \quad (4)$$

where Z_{in} is the input impedance of the absorber, Z_0 is the impedance of free space, $Z_0 = (\mu_0/\varepsilon_0)^{1/2} = 377\ \Omega$, ε_r is the complex permittivity, μ_r is the complex permeability, f is the frequency of the electromagnetic wave, t is the thickness of the single-layer absorber. From equation (3), we can see that the reflection loss $RL = -\infty$, the absorber at $Z_{in}/Z_0 = 1$, which is the strongest absorption peak on the RL-f curve, meaning exhibits zero reflection of the incident electromagnetic wave idealy. The peak frequency of the strongest reflection loss absorption peak is called the perfectly matched frequency (f_p), and the thickness of the absorber is called the perfectly matched thickness (t_p) are called the perfect matched condition.

Figures 10–13 show the exact match conditions and perfect match parameters for the $Y_2Co_{17-x}Fe_x$/PU ($x = 0.0, 1.0, 2.0, 3.0$) absorbers, where, (a) is the frequency f dependence of the quarter wavelengths $\lambda/4$ and three-quarter wavelengths $3\lambda/4$ for the $Y_2Co_{17-x}Fe_x$/PU ($x = 0.0, 1.0, 2.0, 3.0$) absorbers; (b) is the frequency dependence of the impedance match for the corresponding quarter and three-quarter wavelengths and (c) is the perfectly matched parameters for the corresponding absorbers. Figure 10(a) shows the quarter-wavelength thickness and three-quarter thickness of Y_2Co_{17}/PU absorber in relation to frequency. As the frequency increases, the quarter-wavelength thickness and three-quarter thickness gradually decrease. In the range of 1–18 GHz, the quarter wavelength thickness remains between 1 and 8 mm; the three-quarter wavelength thickness remains between 3 and 24 mm. Figure 10(b) shows the impedance versus frequency corresponding to the quarter wavelength of Y_2Co_{17}/PU absorber. We can find that the impedance value corresponding to the quarter wavelength of Y_2Co_{17}/PU absorber decreases with increasing frequency; at 5.58 GHz the impedance value corresponding to the quarter wavelength $Z_{in}/Z_0 = 1$, which means that the impedance of the surface of the absorber and the air is the same so that the incident electromagnetic waves can enter the absorber as much as possible and facilitate the absorption of electromagnetic waves. Based on the impedance $Z_{in}/Z_0 = 1$, corresponding to the phase-matching thickness brought into the transmission line theory, the perfect match parameters are obtained as shown in Figure 10(c). As shown in Figure 10(c) for the complete loss peak of the Y_2Co_{17}/PU absorber, the d size of the strongest reflection value is –92.71 dB, the matching thickness is only 2.441 mm, and the effective bandwidth (–10 dB) is 2.06 GHz. The perfect matching parameters and absorption characteristics of the Y_2Co_{17}/PU absorber are shown in Table 1.

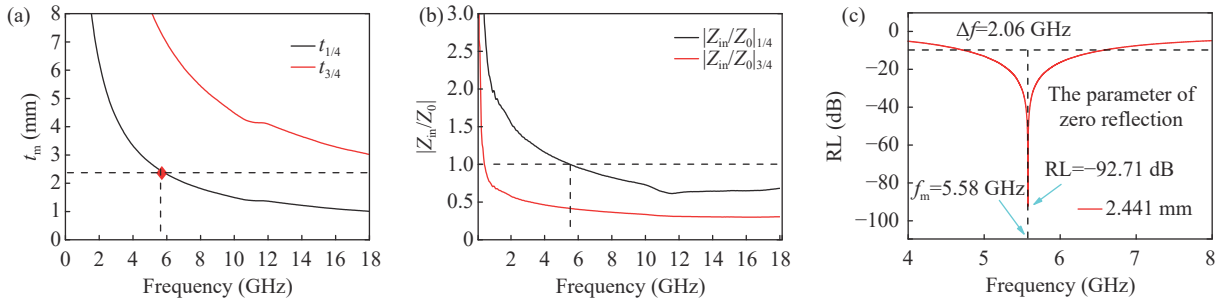

Figure 10 (a) $\lambda/4$ and $3\lambda/4$ values calculated from the complex permittivity and permeability of Y_2Co_{17}/PU compound absorber; (b) Dependence of input resistance on frequency of Y_2Co_{17}/PU compound absorber; (c) Dependence of RL experimental and calculation results on frequency at 2.441 mm for Y_2Co_{17}/PU compound absorber.

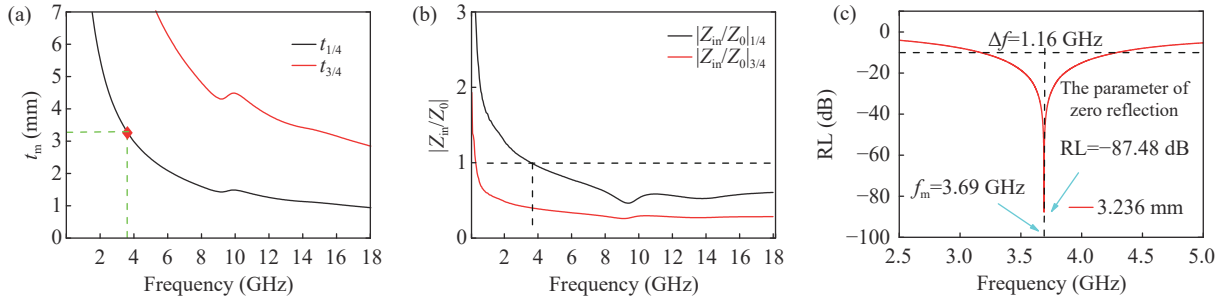

Figure 11 (a) $\lambda/4$ and $3\lambda/4$ values calculated from the complex permittivity and permeability for $Y_2Co_{16}Fe_1$/PU compound absorber; (b) Dependence of input resistance on frequency for $Y_2Co_{16}Fe_1$/PU compound absorber; (c) Dependence of RL experimental and calculation results on frequency at 3.236 mm for $Y_2Co_{16}Fe_1$/PU compound absorber.

In a similar way, a comprehensive analysis of the $Y_2Co_{17-x}Fe_x$/PU absorbers with varying Fe content was car-

ried out for several other absorbers using a combination of this phase matching theory and transmission line theory. The perfect match thickness t was obtained from the impedance $Z_{in}/Z_0 = 1$ and phase matching $t = \frac{c}{4f\sqrt{\varepsilon_r\mu_r}}$, which was carried over to the transmission line theory to also obtain the corresponding perfect reflection loss, as shown in Figures 11–13, respectively. We observe that the strongest reflection loss of $Y_2Co_{16}Fe_1$/PU absorber is −87.48 dB at a thickness of 3.236 mm, with an effective bandwidth 1.16 GHz; the strongest reflection loss of $Y_2Co_{15}Fe_2$/PU absorber is −89.94 dB at a thickness of 4.753 mm, with an effective bandwidth 0.55 GHz; and the strongest reflection loss of $Y_2Co_{14}Fe_3$/PU absorber is −91.68 dB at a thickness of 4.857 mm, with an effective bandwidth 0.45 GHz, respective. The detailed perfect matching conditions and parameters are shown in Tables 2, 3 and 4. It is obvious that as the iron content increases, the perfect match frequency of the reflection loss peak shifts to the lower frequency region, with the perfect match frequency shifting from 5.6 GHz (x=0.0) to 1.80 GHz (x=3.0), which is inextricably connected to the shift of the natural resonance frequency of the $Y_2Co_{17-x}Fe_x$/PU (x=0.0,1.0,2.0,3.0) composites to lower frequencies. In conclusion, this method provides a quick and easy way to analyse the potential performance of absorbing materials compared to most of the performance determination methods provided for absorbing materials.

Meanwhile, it is worth noting also that it has been discovered that for the reflection loss peak of the absorber with

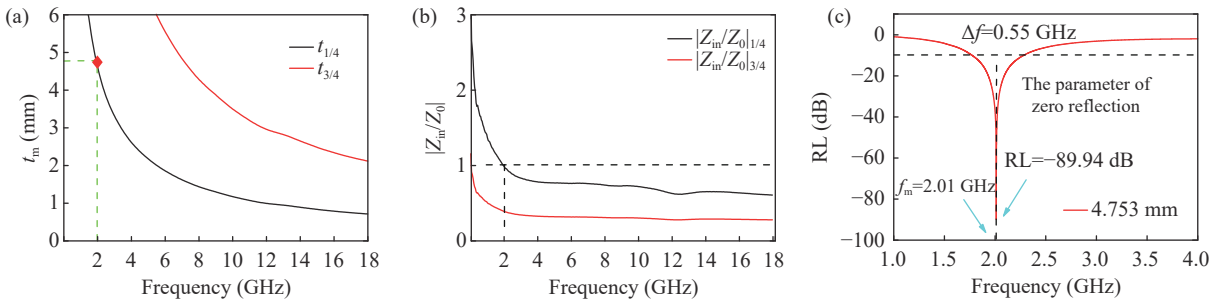

Figure 12 (a) $\lambda/4$ and $3\lambda/4$ values calculated from the complex permittivity and permeability for $Y_2Co_{15}Fe_2$/PU compound absorber; (b) Dependence of input resistance on frequency for $Y_2Co_{15}Fe_2$/PU compound absorber; (c) Dependence of RL experimental and calculation results on frequency at 4.753 mm for $Y_2Co_{15}Fe_2$/PU compound absorber.

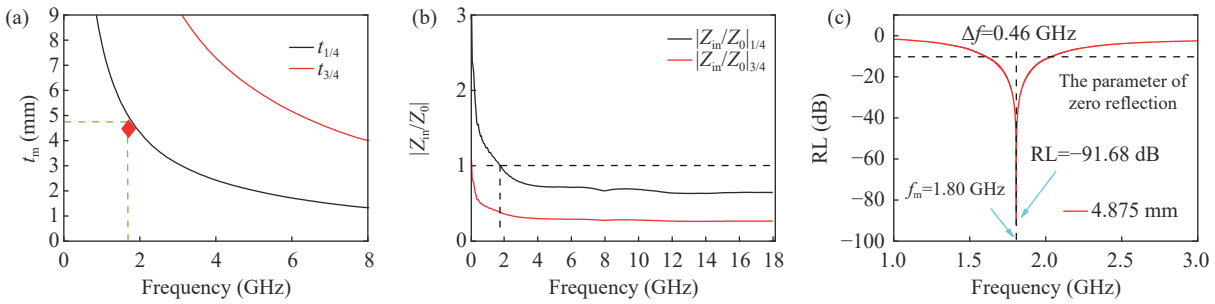

Figure 13 (a) $\lambda/4$ and $3\lambda/4$ values calculated from the complex permittivity and permeability for $Y_2Co_{14}Fe_3$/PU compound absorber; (b) Dependence of input resistance on frequency for $Y_2Co_{14}Fe_3$/PU compound absorber; (c) Dependence of RL experimental and calculation results on frequency at 4.875 mm for $Y_2Co_{14}Fe_3$/PU compound absorber.

Table 1 Zero reflection parameter and Absorption performance at perfect match or Y_2Co_{17}/PU compound absorber.

Matching parameters	μ	ε	$\sqrt{\varepsilon_r/\mu_r}$	$\sqrt{\mu_r\varepsilon_r}$
Parameter value	1.57–0.59i	17.6–0.847i	3.24	5.43
Absorption performance	t_m(mm)	f_m(GHz)	Z_{in}/Z_0	RL(dB)
Parameter value	2.441	5.60	0.995	–92.71

Table 2 Zero reflection parameter and Absorption performance at perfect match for $Y_2Co_{16}Fe_1$/PU compound absorber.

Matching parameter	μ	ε	$\sqrt{\varepsilon_r/\mu_r}$	$\sqrt{\mu_r\varepsilon_r}$
Parameter value	1.73–0.59i	21.2–1.19i	3.41	6.23
Absorption performance	t_m(mm)	f_m(GHz)	Z_{in}/Z_0	RL(dB)
Parameter value	3.236	3.68	0.995	–87.48

Table 3 Zero reflection parameter and Absorption performance at perfect match for $Y_2Co_{15}Fe_2$/PU compound absorber.

Matching parameter	μ	ε	$\sqrt{\varepsilon_r/\mu_r}$	$\sqrt{\mu_r\varepsilon_r}$
Parameter value	1.91–0.532i	30.6–1.87i	3.94	7.80
Absorption performance	t_m (mm)	f_m (GHz)	Z_{in}/Z_0	RL(dB)
Parameter value	4.753	2.02	0.995	–89.94

Table 4 Zero reflection parameter and Absorption performance at perfect match $Y_2Co_{14}Fe_33$/PU compound absorber.

Matching parameter	μ	ε	$\sqrt{\varepsilon_r/\mu_r}$	$\sqrt{\mu_r\varepsilon_r}$
Parameter value	1.93–0.484i	36.3–2.12i	4.27	8.50
Absorption performance	t_m (mm)	f_m (GHz)	Z_{in}/Z_0	RL(dB)
Parameter value	4.875	1.80	0.996	–91.68

a large reflection loss value RL, the $\sqrt{\varepsilon_r/\mu_r}$ of the complex electromagnetic parameter of the absorber at the perfect matching frequency point is between 2 and 5. For example in this paper the $\sqrt{\varepsilon_r/\mu_r}$ = 3.24 for Y_2Co_{17}/PU absorber, $\sqrt{\varepsilon_r/\mu_r}$ = 3.41 for $Y_2Co_{16}Fe_1$/PU absorbers, $\sqrt{\varepsilon_r/\mu_r}$ = 3.94 for $Y_2Co_{15}Fe_2$/PU absorbers and $\sqrt{\varepsilon_r/\mu_r}$ = 4.27 for $Y_2Co_{14}Fe_3$/PU absorbers. In this case, we also observed that the reflection loss value corresponding to the reflection loss peak varies with frequency and the quarter wavelength thickness varies with frequency in the similar trend as shown in Figure 14, where Figures 14(a)–(d) show the color plot of reflection loss RL versus frequency f and composite thickness d for the $Y_2Co_{17-x}Fe_x$/PU absorbers with different amount of Fe replacement, and Figures 14(e)–(g) show the quarter wavelength thickness varies with frequency for the $Y_2Co_{17-x}Fe_x$ with different amount of Fe replacement.

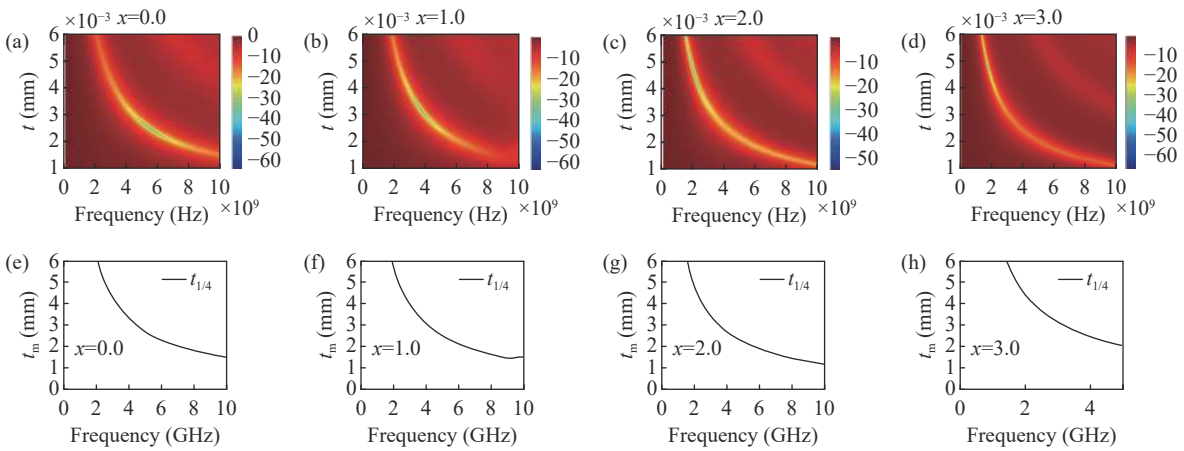

Figure 14 (a)–(d) The color plot of reflection loss RL versus frequency f and composite thickness d for $Y_2Co_{17-x}Fe_x$/PU absorbers with different amount of iron replacement; (e)–(g) Show the quarter wavelength thickness varies with frequency for $Y_2Co_{17-x}Fe_x$ with different amount of Fe replacement.

4. Application prospect study of $Y_2Co_{17-x}Fe_x$/PU absorbers

As an ideal absorber, the incident wave should be attenuated by the absorber as much as possible. The electromagnetic energy loss in the absorber is the difference between the energy of the incident and reflected waves in the case of energy conservation. This is usually directly related to the electromagnetic parameters of the absorber. The replacement of Fe has no significant effect on the magnitude of the magnetic permeability of $Y_2Co_{17-x}Fe_x$/PU (x = 0.0, 1.0, 2.0, 3.0), but there is a significant decrease in the permittivity. According to (2), it is not only significantly reduces the thickness of the absorber, but also facilitates the impedance matching.

The frequency dependence of RL for the $Y_2Co_{17-x}Fe_x$ composite absorbers with various Fe content (x = 0.0, 1.0, 2.0, 3.0) are shown in Figure 15. Figures 15(a)–(d) show the typical dependence of RL on frequency and thickness for $Y_2Co_{17-x}Fe_x$ composite absorbers with different Fe substitution over the measurement range. It is obvious that there is a significant of RL and operating frequencies between the absorbers of the different Fe substitutes. Each absorber has unique electromagnetic absorption properties and the three-dimensional projection of individual absorbers gives a strong indication of the combined microwave absorption properties of the absorbers. It is worth noting that the bright

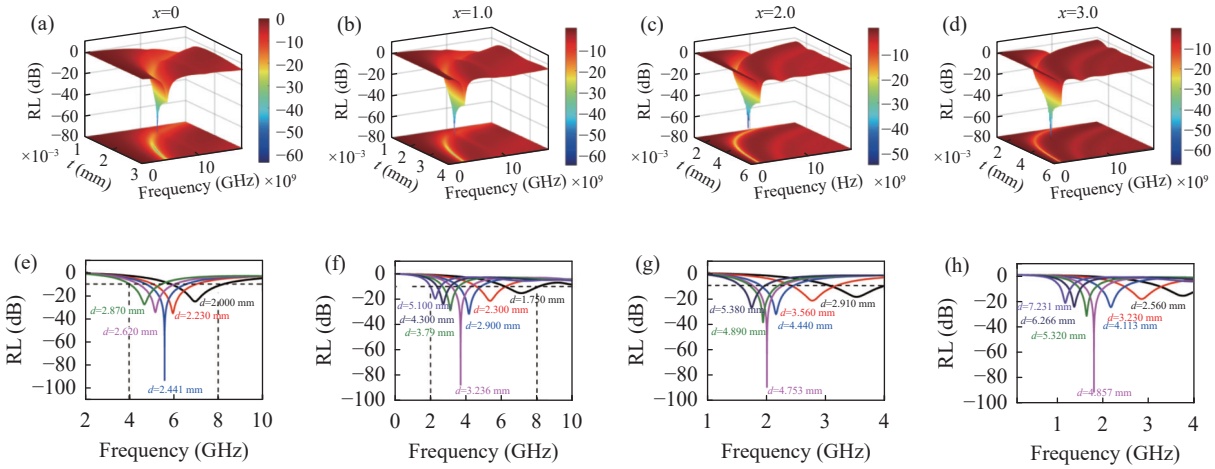

Figure 15 (a)–(d) The color plot of reflection loss RL versus frequency f and composite thickness d for $Y_2Co_{17-x}Fe_x$/PU absorbers with different amount of Fe replacement; (e)–(g) Show the quarter wavelength thickness varies with frequency for $Y_2Co_{17-x}Fe_x$ with different amount of Fe replacement.

bars in the 3D projection move towards lower frequencies as the amount of Fe substitution increases, which helps to address the "thin" and "low frequency" issues in the field of microwave absorption. In Figures 15(e)–(h), the RL curves are shown for different thicknesses of the composite with different iron substitutes when working as a single layer absorber alone. As the thickness increases, the absorption peak moves towards the lower frequencies and the value of the reflection loss RL first decreases to a minimum, meaning that a perfect reflection loss is obtained when the perfectly matched thickness peaks and then increases again.

For practical applications, the selection of absorbing materials needs to take into account the matching thickness, microwave absorption bandwidth and the applied frequency band, rather than just discussing the value of the peak reflection loss. Figures 15(e)–(g) show the reflection loss (RL)–frequency (f) relationship for the same volume fraction with different Fe replacement. In Figure 15(e), it is demonstrated that the Y_2Co_{17}/PU absorber has a minimum RL of −92.71 dB at 5.60 GHz and a thickness of 2.441 mm, where the impedance $|Z_{in}/Z_0|$ equals 1. All the values of RL are below −10 dB with the thickness of the sample in the range of 2–2.87 mm. which is convenient for practical applications in the band (4–8 GHz). Similarly, in Figure 15(f), the $Y_2Co_{16}Fe_1$/PU absorber is still applicable to the C-band, but the RL has been enhanced significantly and the thickness of the absorber has been decreased markedly, from a full coverage of 2–2.85 mm without Fe replacement to a full coverage of 1.75–2.80 mm at present. It is particularly relevant to note that the $Y_2Co_{15}Fe_2$/PU composite absorber shows a significant effect in the S-band. In the C-band, the reflection loss has a maximum value of −37 dB when thickness of the $Y_2Co_{15}Fe_2$/PU composite absorber is 3.79 mm, with a frequency at 3.3 GHz, when the effective bandwidth is 1 GHz (3–4 GHz).The s radar band is mainly used to detect airborne targets at medium and long distances, for satellite communications and weather forecasting, and also for 5G communications. If put into practical application, it will effectively change people's lives.

The L-band radar detection system is a high altitude detection system developed independently by China, featuring a high degree of automation, very fast timeliness, high accuracy, ease of use and a novel interface. Radar devices operating in this band are susceptible to interference from external electromagnetic signals, however, due to their low operating frequency, it is difficult for general wave absorbing materials to fulfil their shielding tasks. Fortunately, the perfectly matched frequency of the $Y_2Co_{14}Fe_3$/PU composite absorber is shifted towards the L-band with a strongest reflection loss RL of −91.68 dB; between 3.2 and 5.1 mm, all RL values are below −10 dB as shown in Figure 15(h). The $Y_2Co_{14}Fe_3$/PU composite absorbing material has an effective absorption bandwidth of 300 MHz (1.5–1.8GHz) at a thickness of 5.230 mm, while it can absorb the full L-band at −4 dB. The $Y_2Co_{14}Fe_3$/PU composite absorbers is potential candidates for L-band radar wave absorption, which was rarely reported.

IV. Conclusion

In summary, high purity Y_2Co_{17} alloy compounds were synthesised via a low-cost reductive diffusion process, and similarly, the replacement of Co atoms with Fe atoms afforded high purity $Y_2Co_{17-x}Fe_x$ alloys compounds. The crystal structure and intrinsic magnetic properties of the Fe substituted $Y_2Co_{17-x}Fe_x$ alloys compounds were investigated, and the high frequency properties of the polyurethane composites. It was discovered that the substitution of the Fe atom for a Co atom results in greater crystal lattice parameters and cell parameters, which produces a saturation magnetization intensity M_s and significantly alters the magnetic characteristics. Additionally, we investigated $Y_2Co_{17-x}Fe_x$/Pu absorbers with different Fe contents based on the combination of phase matching theory and the transmission line theory. With varied Fe replacements in the same volume fraction, the results demonstrate that all $Y_2Co_{17-x}Fe_x$/Pu absorbers have outstanding absorption performance (reflec-

tion loss less than −85 dB), which is consistent with the results confirmed by the interfacial reflection model. The measurements of the absorption of radar waves reveal that the variance of the reflection loss with increasing iron concentration is comparable with the variation of the magnetic material's natural frequency. According to the combined conclusion, Y_2Co_{17}/PU absorber and $Y_2Co_{16}Fe_1$/PU absorber are excellent options in the S-band, and $Y_2Co_{15}Fe_2$/PU absorber and $Y_2Co_{14}Fe_3$/PU absorber are excellent candidates in the C-band.

Acknowledgements

This work was supported by the National Key Research and Development Program of China (Grant No. 2021YFB350 1302), the National Natural Science Foundation of China (Grant No. 51731001), and the Fund from the State Key Laboratory of Baiyunobo Rare Earth Resource Researches and Comprehensive Utilization's Key Research and Development Projects.

References

[1] Y. L. Wang, P. Y. Zhao, B. L. Liang, *et al*., "Carbon nanotubes decorated Co/C from ZIF-67/melamine as high efficient microwave absorbing material," *Carbon*, vol. 202, pp. 66–75, 2023.

[2] X. Li, M. H. Li, X. Lu, *et al*., "A sheath-core shaped ZrO2-SiC/SiO_2 fiber felt with continuously distributed SiC for broad-band electromagnetic absorption," *Chemical Engineering Journal*, vol. 419, article no. 129414, 2021.

[3] F. Chen, S. S. Zhang, B. B. Ma, *et al*., "Bimetallic CoFe-MOF@$Ti_3C_2T_x$ MXene derived composites for broadband microwave absorption," *Chemical Engineering Journal*, vol. 431, article no. 134007, 2022.

[4] H. Wang, L. Qiao, Z. Y. Zheng, *et al*., "Microwave absorption properties regulation and bandwidth formula of oriented $Y_2Fe_{17}N_{3-\delta}$@SiO_2/PU composite synthesized by reduction–diffusion method," *Chinese Physics B*, vol. 31, no. 11, article no. 114206, 2022.

[5] X. M. Zhang, Y. Liu, Z. Y. Liu, *et al*., "Microwave absorption properties of nanocrystalline $Ni_{1-x}Zn_xFe_2O_4$ synthesized by spraying-coprecipitation method," *Journal of Magnetism and Magnetic Materials*, vol. 560, article no. 169647, 2022.

[6] X. Y. Wang, Y. Liang, S. C. Wei, *et al*., "Preparation and absorbing property analysis of ZnO-doped magnetic graphene composite material," *Journal of Magnetism and Magnetic Materials*, vol. 556, article no. 169450, 2022.

[7] Y. Q. Wang, H. G. Wang, J. H. Ye, *et al*., "Magnetic CoFe alloy@C nanocomposites derived from ZnCo-MOF for electromagnetic wave absorption," *Chemical Engineering Journal*, vol. 383, article no. 123096, 2020.

[8] H. L. Peng, Z. Q. Xiong, Z. H. Gan, *et al*., "Microcapsule MOFs@MOFs derived porous "nut-bread" composites with broadband microwave absorption," *Composites Part B:Engineering*, vol. 224, article no. 109170, 2021.

[9] M. H. Li, X. R. Song, J. M. Xue, *et al*., "Construction of hollow carbon nanofibers with graphene nanorods as Nano- antennas for lower-frequency microwave absorption," *ACS Applied Materials & Interfaces*, vol. 15, no. 26, pp. 31720–31728, 2023.

[10] F. Chen, H. Luo, Y. Z. Cheng, *et al*., "Nickel/Nickel phosphide composite embedded in N-doped carbon with tunable electromagnetic properties toward high-efficiency microwave absorption," *Composites Part A:Applied Science and Manufacturing*, vol. 140, article no. 106141, 2021.

[11] H. X. Zhang, Z. R. Jia, A. L. Feng, *et al*., "Enhanced microwave absorption performance of sulfur-doped hollow carbon microspheres with mesoporous shell as a broadband absorber," *Composites Communications*, vol. 19, pp. 42–50, 2020.

[12] X. S. Gu, G. G. Tan, S. W. Chen, *et al*., "Microwave absorption properties of planar-anisotropy $Ce_2Fe_{17}N_{3-\delta}$ powders/Silicone composite in X-band," *Journal of Magnetism and Magnetic Materials*, vol. 424, pp. 39–43, 2017.

[13] G. H. He, Y. P. Duan, and H. F. Pang, "Microwave absorption of crystalline Fe/MnO@C nanocapsules embedded in amorphous carbon," *Nano-Micro Letters*, vol. 12, no. 1, article no. 57, 2020.

[14] H. Y. Wang, X. B. Sun, S. H. Yang, *et al*., "3D ultralight hollow NiCo Compound@MXene composites for tunable and high-efficient microwave absorption," *Nano-Micro Letters*, vol. 13, no. 1, article no. 206, 2021.

[15] S. Zhang, J. T. Wu, W. H. Liang, *et al*., "Flexible and multifunctional polyimide-based composite films by self-reducing reaction for electromagnetic interference shielding in extreme environments," *Carbon*, vol. 212, article no. 118103, 2023.

[16] H. Luo, B. B. Ma, F. Chen, *et al*., "Construction of hollow core-shelled nitrogen-doped carbon-coated yttrium aluminum garnet composites toward efficient microwave absorption," *Journal of Colloid and Interface Science*, vol. 622, pp. 181–191, 2022.

[17] Z. Y. Zheng, Y. G. Ma, H. Wang, *et al*., "Preparation of $Ce_2Fe_{17}N_{3-\delta}$@$FePO_4$ composite with excellent microwave absorption performance by reduction-diffusion (R/D) and phosphating processes," *Journal of Rare Earths*, vol. 41, no. 11, pp. 1754–1762, 2023.

[18] Y. Song, F. X. Yin, C. W. Zhang, *et al*., "Three- dimensional ordered mesoporous carbon spheres modified with ultrafine zinc oxide nanoparticles for enhanced microwave absorption properties," *Nano-Micro Letters*, vol. 13, no. 1, article no. 76, 2021.

[19] H. Y. Wang, X. B. Sun, Y. Xin, *et al*., "Ultrathin self-assembly MXene/Co-based bimetallic oxide heterostructures as superior and modulated microwave absorber," *Journal of Materials Science & Technology*, vol. 134, pp. 132–141, 2023.

[20] M. H. Li, W. J. Zhu, X. Li, *et al*., "$Ti_3C_2T_x$/MoS_2 self- rolling rod-based foam boosts interfacial polarization for electromagnetic wave absorption," *Advanced Science*, vol. 9, no. 16, article no. 2201118, 2022.

[21] H. Luo, B. B. Ma, F. Chen, *et al*., "Bimetallic oxalate rod-derived NiFe/Fe_3O_4@C composites with tunable magneto-dielectric properties for high-performance microwave absorption," *The Journal of Physical Chemistry C*, vol. 125, no. 44, pp. 24540–24549, 2021.

[22] S. T. Gao, Y. C. Zhang, H. L. Xing, *et al*., "Controlled reduction synthesis of yolk-shell magnetic@void@C for electromagnetic wave absorption," *Chemical Engineering Journal*, vol. 387, article no. 124149, 2020.

[23] B. W. Guan, D. H. Ding, L. F. Wang, *et al*., "The electromagnetic wave absorbing properties of cement-based composites using natural magnetite powders as absorber," *Materials Research Express*, vol. 4, no. 5, article no. 056103, 2017.

[24] Y. K. Wang, Z. C. Lin, Z. Liu, *et al*., "The microwave absorption properties of $Fe_{16}N_2$ nanoparticles," *IEEE Transactions on Magnetics*, vol. 58, no. 2, pp. 1–4, 2022.

[25] M. Green and X. B. Chen, "Recent progress of nanomaterials for microwave absorption," *Journal of Materiomics*, vol. 5, no. 4, pp. 503–541, 2019.

[26] F. B. Meng, H. G. Wang, F. Huang, *et al*., "Graphene-based microwave absorbing composites: A review and prospective," *Composites Part B:Engineering*, vol. 137, pp. 260–277, 2018.

[27] Q. Li, Z. Zhang, L. P. Qi, *et al*., "Toward the application of high frequency electromagnetic wave absorption by carbon nanostructures," *Advanced Science*, vol. 6, no. 8, article no. 1801057, 2019.

[28] B. B. Ma, F. Chen, Y. Z. Cheng, *et al*., "$Ti_3C_2T_x$ MXene@NiFe layered double hydroxide derived multiple interfacial composites with efficient microwave absorption," *Journal of Alloys and Compounds*, vol. 936, article no. 168162, 2023.

[29] J. L. Snoek, "Dispersion and absorption in magnetic ferrites at frequencies above one Mc/S," *Physica*, vol. 14, no. 4, pp. 207–217, 1948.

[30] K. Wang, H. Zhang, Y. D. Huang, *et al*., "High-frequency magnetic properties of biphase $Ce_2Fe_{17}N_3/\alpha$-Fe microflakes with easy-plane anisotropy," *Journal of Rare Earths*, vol. 42, no. 1, pp. 110–115, 2024.

[31] Y. F. Sheng, C. F. Tu, P. Wu, *et al*., "Effect of Ni substitution on magnetic properties and microwave absorption of the Y_2Co_{17} compounds and composites," *Journal of Applied Physics*, vol. 134, no. 17, article no. 173901, 2023.

[32] T. Maeda, S. Sugimoto, T. Kagotani, *et al*., "Effect of the soft/hard exchange interaction on natural resonance frequency and electromagnetic wave absorption of the rare earth–iron–boron compounds," *Journal of Magnetism and Magnetic Materials*, vol. 281, no. 2-3, pp. 195–205, 2004.

[33] L. X. Lian, L. J. Deng, M. Han, *et al*., "Microwave electromagnetic and absorption properties of $Nd_2Fe_{14}B/\alpha$-Fe nanocomposites in the 0.5–18 and 26.5–40GHz ranges," *Journal of Applied Physics*, vol. 101, no. 9, article no. 09M520, 2007.

[34] J. B. Yang, W. Y. Yang, F. S. Li, *et al*., "Research and development of high-performance new microwave absorbers based on rare earth transition metal compounds: A review," *Journal of Magnetism and Magnetic Materials*, vol. 497, article no. 165961, 2020.

[35] S. V. Trukhanov, A. V. Trukhanov, M. M. Salem, *et al*., "Preparation and investigation of structure, magnetic and dielectric properties of $(BaFe_{11.9}Al_{0.1}O_{19})_{1-x}$ - $(BaTiO_3)_x$ bicomponent ceramics," *Ceramics International*, vol. 44, no. 17, pp. 21295–21302, 2018.

[36] G. Y. Qiao, Q. W. Hu, P. Y. Zhang, *et al*., "The effect of samarium substitution on magnetic properties and microwave absorption of the rare earth-iron-boron compounds and composites," *Journal of Alloys and Compounds*, vol. 825, article no. 154179, 2020.

[37] G. Y. Qiao, W. Y. Yang, Y. F. Lai, *et al*., "Crystal structure, magnetic and microwave absorption properties of $Ce_{2-x}Sm_xFe_{17}N_{3-\delta}$/paraffin composites," *Materials Research Express*, vol. 6, no. 1, article no. 016103, 2018.

[38] W. Y. Yang, Y. F. Zhang, G. Y. Qiao, *et al*., "Tunable magnetic and microwave absorption properties of $Sm_{1.5}Y_{0.5}Fe_{17-x}Si_x$ and their composites," *Acta Materialia*, vol. 145, pp. 331–336, 2018.

[39] Z. H. Ma, T. L. Zhang, and C. B. Jiang, "A facile synthesis of high performance $SmCo_5$ nanoparticles," *Chemical Engineering Journal*, vol. 264, pp. 610–616, 2015.

[40] C. F. Tu, Z. Y. Zheng, L. Qiao, *et al*., "Mechanism of radar wave absorption and bandwidth for easy-plane Y_2Co_{17} rare earth soft magnetic composites," *Acta Physcica Sinica*, vol. 71, no. 18, article no. 184201, 2022.

[41] Y. C. Chang, J. Jiang, and Y. C. Chuang, "Mössbauer effect study of $Y_2(Co_{1-x}Fe_x)_{17}$ compounds," *Journal of the Less Common Metals*, vol. 107, no. 1, pp. 1–9, 1985.

[42] D. Jiles, *Introduction to Magnetism and Magnetic Materials*, 3rd ed., CRC Press, Boca Raton, 2015.

[43] J. P. Zhong, G. G. Tan, Q. K. Man, *et al*., "Optimisation of microwave absorption properties of Fe-substituted $Y_2Co_{17-x}Fe_x$ soft-magnetic composites," *Journal of Materials Science:Materials in Electronics*, vol. 32, no. 23, pp. 27849–27859, 2021.

[44] D. S. Xue, F. S. Li, X. L. Fan, *et al*., "Bianisotropy picture of higher permeability at higher frequencies," *Chinese Physics Letters*, vol. 25, no. 11, pp. 4120–4123, 2008.

[45] S. Zhang, T. Wang, M. Z. Gao, *et al*., "Strict proof and applicable range of the quarter-wavelength model for microwave absorbers," *Journal of Physics D:Applied Physics*, vol. 53, no. 26, article no. 265004, 2020.

Chengfa Tu was born in Chongqing, China. He graduated from Inner Mongolia University with the B.S. degree in 2021, and is currently the M.S. candidate at Lanzhou University, Lanzhou, China. His current research interests include rare earth-transition metal soft magnetic materials and radar wave absorbing materials.
(Email: tuchf21@lzu.edu.cn)

Liang Qiao was born in 1981. Now he is a M.S. Supervisor, and Associate Professor in College of Physical Science and Technology, Lanzhou University. He is currently working in the Institute of Applied Magnetism, Key Laboratory of Magnetism and Magnetic Materials of the Ministry of Education, Lanzhou University. He has been devoted to the research of magnetism and high-frequency magnetic materials since he was a graduate student, and has successively engaged in the analysis of Mussburger spectral orientation, and the establishment of multi-physics field coupling model integrating Maxwell's equations and Landau-Lifshitz equations. Currently, he is committed to the research and development of new high-frequency soft magnetic materials for switching power supply devices and high-performance electromagnetic wave absorbing materials. He has presided over one sub-topic of the major project of the National Natural Foundation of China, and participated in many projects of the National Key Special Project and the National Natural Science Foundation of China.
(Email: qiaoliang@lzu.edu.cn)